

Distribution Agreement

In presenting this thesis as a partial fulfillment of the requirements for a degree from Emory University, I hereby grant to Emory University and its agents the non-exclusive license to archive, make accessible, and display my thesis in whole or in part in all forms of media, now or hereafter now, including display on the World Wide Web. I understand that I may select some access restrictions as part of the online submission of this thesis. I retain all ownership rights to the copyright of the thesis. I also retain the right to use in future works (such as articles or books) all or part of this thesis.

Vu Ngo

March 9, 2023

Structural interactions of human respiratory syncytial virus NS2 with
human innate immune system receptors RIG-I and MDA5

by

Vu Ngo

Dr. Bo Liang, PhD

Adviser

Biology

Dr. Bo Liang, PhD

Adviser

Dr. Jitendra Thakur, PhD

Committee Member

Dr. Matthew Gardner, PhD

Committee Member

2023

Structural interactions of human respiratory syncytial virus NS2 with
human innate immune system receptors RIG-I and MDA5

By

Vu Ngo

Dr. Bo Liang, PhD

Adviser

An abstract of
a thesis submitted to the Faculty of Emory College of Arts and Sciences
of Emory University in partial fulfillment
of the requirements of the degree of
Bachelor of Science with Honors

Biology

2023

Abstract

Structural interactions of human respiratory syncytial virus NS2 with human innate immune system receptors RIG-I and MDA5

By Vu Ngo

Respiratory syncytial virus (RSV) is a significant public health threat that causes severe bronchitis and pneumonia in children and immunocompromised individuals. In response to RSV infection, host cells employ various pattern recognition receptors (PRR). These include receptors of the retinoic acid-inducible gene I-like receptors family (RLR) of the innate immune system. retinoic acid-inducible gene I (RIG-I) and melanoma differentiation-associated gene 5 (MDA5) are two such RLRs that detect cytosolic viral RNA. RSV has 10 genes that code for 11 proteins, including nonstructural protein 2 (NS2) which plays an important role in antagonizing human type I interferon (IFN) response through direct interaction with RIG-I at its caspase recruitment domains (CARD). NS2 is also found to interact with MDA5 in its inactive conformation. Despite these insights into the molecular mechanism of NS2 antagonism, definite structures of the direct interactions of NS2 with the two RLR are not established. In order to address this knowledge gap, we aim to solve the structure of the direct interactions of NS2 with RIG-I and MDA5. First, we optimized an in vitro expression system using *E. coli* to express recombinant NS2, RIG-I, and MDA5 with a His-MBP tag. We also expressed the CARDS of RIG-I and MDA5 along with our tags in order to examine possible interaction at the domains. The recombinant proteins were purified using Ni-NTA affinity column, ion exchange column, and size exclusion columns. Purified NS2 and MDA5 CARDS were used in pre-crystallization tests to determine suitable conditions of crystallization of the complex between NS2 and MDA5 CARDS.

Structural interactions of human respiratory syncytial virus NS2 with
human innate immune system receptors RIG-I and MDA5

By

Vu Ngo

Dr. Bo Liang, PhD

Adviser

A thesis submitted to the Faculty of Emory College of Arts and Sciences
of Emory University in partial fulfillment
of the requirements of the degree of
Bachelor of Science with Honors

Biology

2023

Acknowledgements

I am thankful to Dr. Liang for being a wonderful advisor for the past year. His guidance and patience taught me many things about the skills and professionalism of a researcher. I would like to thank Dr. Zhenhang Chen for teaching me the techniques and experimental planning required to carry out the project. In addition, I would like to thank Eliseo Salas, a current PhD student at Emory, for working with me on the project. He is not only a great collaborator who devotes all of his time to the project but is also a great teacher who teaches me about experimental design and techniques. Special thanks to Dylan Blohm, the best lab assistant, who helped me with random questions I have about techniques and made the time in my lab a lot more enjoyable. I look up to every mentioned individual as they are models for the type of scientist I strive to be.

A final thanks to my family for supporting my journey, Dr. Jitendra Thakur, and Dr. Matthew Gardner for taking their time to be in my committee, and all undergraduate students of the Liang lab for making my time in the lab more enjoyable.

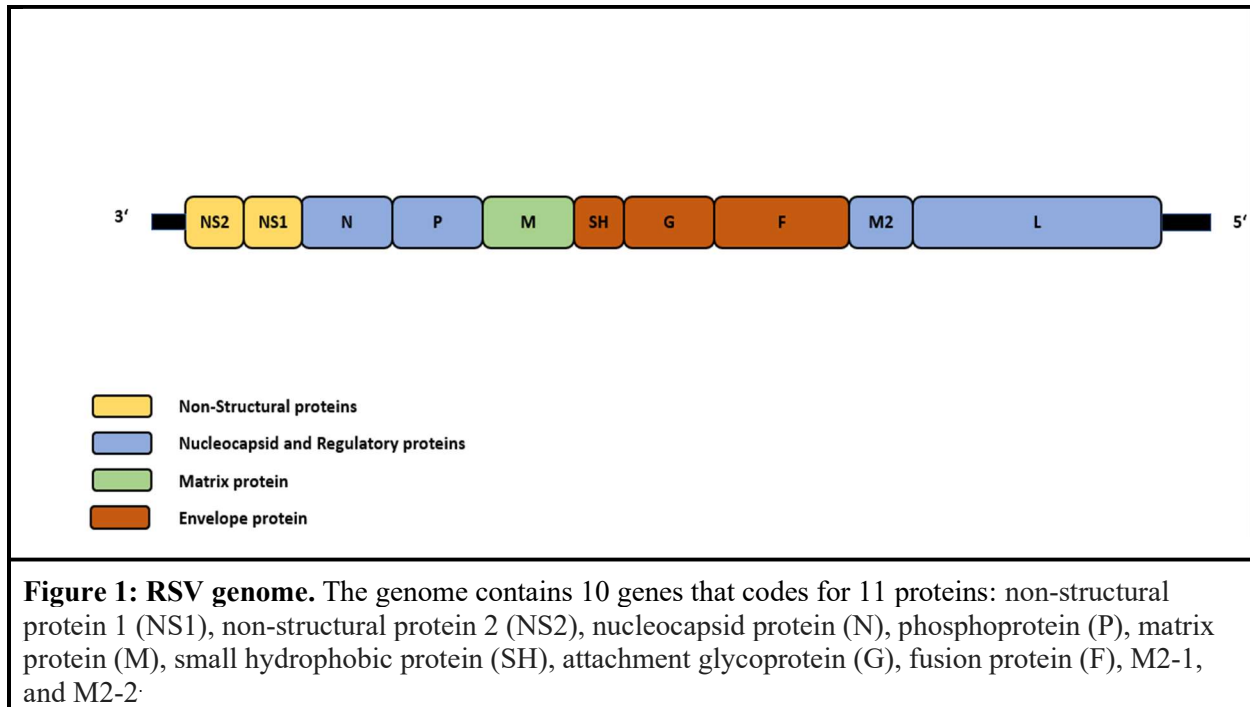
Table of Contents

Introduction	1
Results	5
MDA5 full length purification.....	5
MDA5 CARDS purification... ..	10
NS2-MBP purification.....	13
Crystal Conditions Screening	17
Discussion	18
Material and method	20
Cells and Plasmids.....	20
Transformation.....	21
Protein expression.....	21
Protein purification.....	21
References	23

Introduction

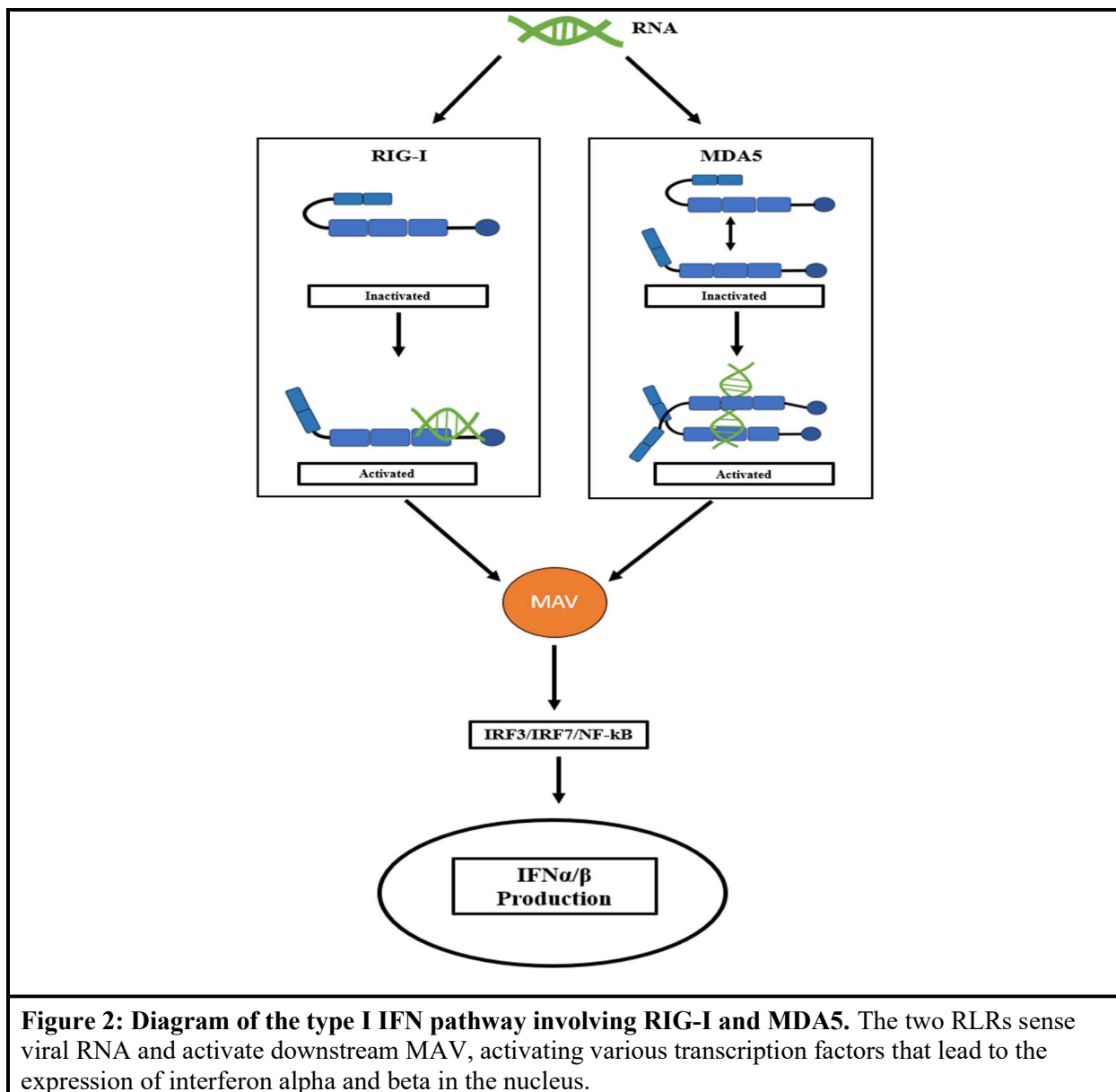
Respiratory syncytial virus (RSV) is a common non-segmented, negative-strand RNA virus of the Pneumoviridae family. Upon infection in humans, RSV causes mild cold-like symptoms. However, children and those with a weakened immune system are susceptible to severe infection cases, which can result in bronchitis and pneumonia. Currently, RSV is the number one cause of bronchitis and pneumonia in children under the age of 1 in the US with an estimated 58,000-80,000 cases of hospitalization every year⁽¹⁾. With no dedicated treatment available, RSV poses a great challenge to the nation's public health.

RSV genome contains 10 genes that code for 11 proteins (Figure 1)⁽⁴⁾. The first two genes encode for nonstructural protein 1 (NS1) and nonstructural protein 2 (NS2). These two proteins play key roles in the suppression of human immune response. In RSV infected mice, NS1 and NS2 reduce cytotoxic T lymphocytes response by suppressing type I interferon response (IFN)⁽⁵⁾. In vitro cultures, NS1 and NS2 blocks beta interferon signaling^(6, 7). Cooperatively, they can enable resistance against interferon responses⁽⁸⁾. NS1 and NS2 effectively suppress the induction and the effects of IFN responses by targeting various key receptor proteins of the innate immune system.



As the first line of defense, the human innate immune system relies on various pattern recognition receptors (PRRs) to detect pathogen derived molecules also known as pathogen-associated molecular patterns (PAMP). Detection of PAMPs by PRRs results in the activation of various immune pathways. One of which is the type I interferon response of the innate immune system. Two important cytosolic PRRs responsible for eliciting type I IFN are the retinoic acid-inducible gene-1 (RIG-I) and melanoma differentiation-associated gene 5 (MDA5). The structures of these two receptors share many similarities as they include: two caspase recruitment domains (CARD) at their N-terminus; two helicase domains made of Hel1, Hel2i, and Hel2; a C-terminal domain (CTD) as reviewed by Onotomo et al ⁽³⁾. RIG-I and MDA5 are RLRs responsible for the detection of viral RNA in the cytosol. RIG-I exists in an inactive, autorepressed state. In this conformation, the two CARDS interact with Hel2i of the helicase domains and become unavailable for downstream signaling ⁽⁹⁾. RIG-I detects viral blunt-ended double-stranded RNA of around 20 base pairs or single-stranded RNA with 5'-phosphates

through the CTD and the helicase domains^(10–12, 15). Upon binding of viral RNA, CARDs are released and become available for signaling with downstream mitochondrial antiviral signaling protein (MAVS), which activates several transcription factors such as IRF3 and IRF7 that modulate expressions of many IFN-stimulated genes (ISG). MDA5 is proposed to exist in a conformational equilibrium between an open form and a closed form⁽¹³⁾. The latter is favored when the receptor is in a ligand-free state. Unlike RIG-I, MDA5 senses viral RNA through cooperative formation of MDA5 filaments along viral double stranded RNA^(13, 14). On the outside of these filaments lay arrays of CARDs that interact with MAV CARDs for downstream signaling (Figure 2)^(13, 15).



RIG-I and MDA5 play a dominant role in RSV infections. Knockdown experiments of RIG-I using small interfering RNA prevent activations of interferon response factor 3 (IRF3) and nuclear factor- κ B (NF- κ B), which are important transcription factors for the expression of IFN type I genes⁽¹⁶⁾. Expression of RIG-I and MDA5 is upregulated in children infected by RSV⁽¹⁷⁾. Previous studies show that NS2 is a potent disruptor of RIG-I and MDA5 immune functions. NS2 interferes with beta interferon transcription through its binding to RIG-I N-terminal CARDs

(2). A recent structure study shows NS2 interacts with inactive conformation of RIG-I and MDA5⁽¹⁸⁾. These findings suggest that RIG-I and MDA5 are antagonized through direct binding of NS2, inhibiting host immune responses. Despite the progress made in understanding the molecular mechanisms of NS2 antagonism, we still lack a definite structure of the supposed direct interaction of NS2 with RIG-I and MDA5. In order to resolve this gap in knowledge, we propose to solve the structure of the direct interactions of NS2 with RIG-I and MDA5.

In this study, we optimized an expression system using *E. coli* to express human RSV NS2, RIG-I, MDA5, and MDA5 CARDS. We purify expressed proteins using affinity columns. Upon successful purifications, we create complexes between NS2 with each of two human immune receptors as well as with the CARDS truncation of MDA5. We then test the complexes in multiple crystal screening conditions in an attempt to optimize the conditions for crystal formation of the complexes.

Result

MDA5 full length purification

Ni-NTA Column

We started first with MDA5 full length due to plasmid availability. Initially, we used Ni-NTA column to purify the protein using His-tag's affinity to the resin. The column showed positive results as SDS-PAGE gel results showed MDA5 full length with His-tag (120 kDa) elutes at 100mM, 300mM and 500mM imidazole concentration (Figure 3). However, the fractions contained most MDA5 at 300mM imidazole concentration still have many contaminants especially at 75 kDa. The lack of bands in the wash fractions indicate that the contaminant bands in the elution fractions are not unspecific binding proteins. The presence of MDA5 full length band in the pellet sample suggests that some of the protein was denatured during sonication and precipitated into the pellet during centrifugation. This could explain the lack of an intense MDA5 full length band in the supernatant sample (L). Elution fractions of 300mM imidazole concentration were collected and diluted 10 times to a final imidazole concentration of 30mM and a final NaCl concentration of 50mM. This step was needed to prepare the sample for further purification using Heparin Column, which is designed for purification of RNA/DNA binding proteins.

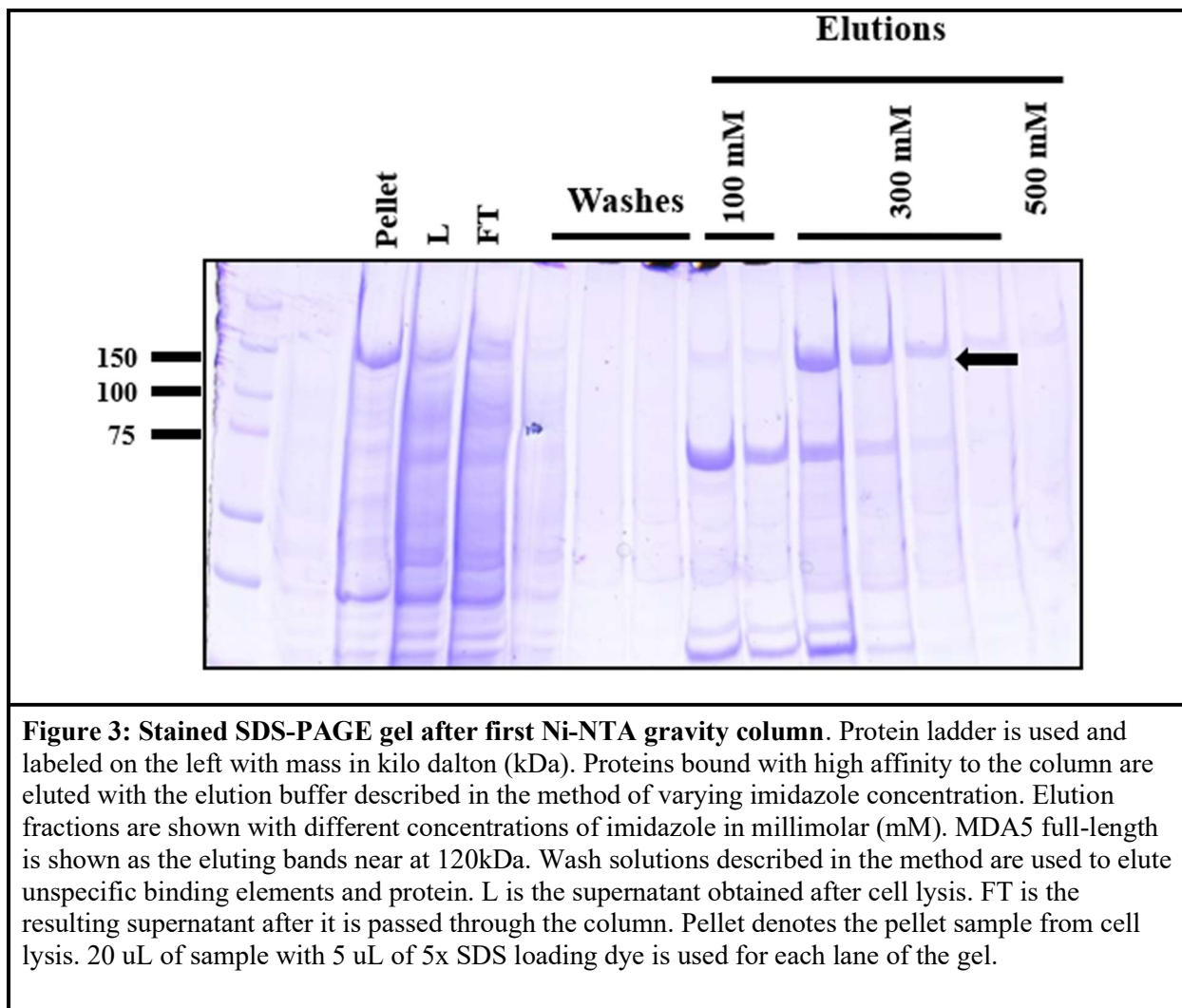
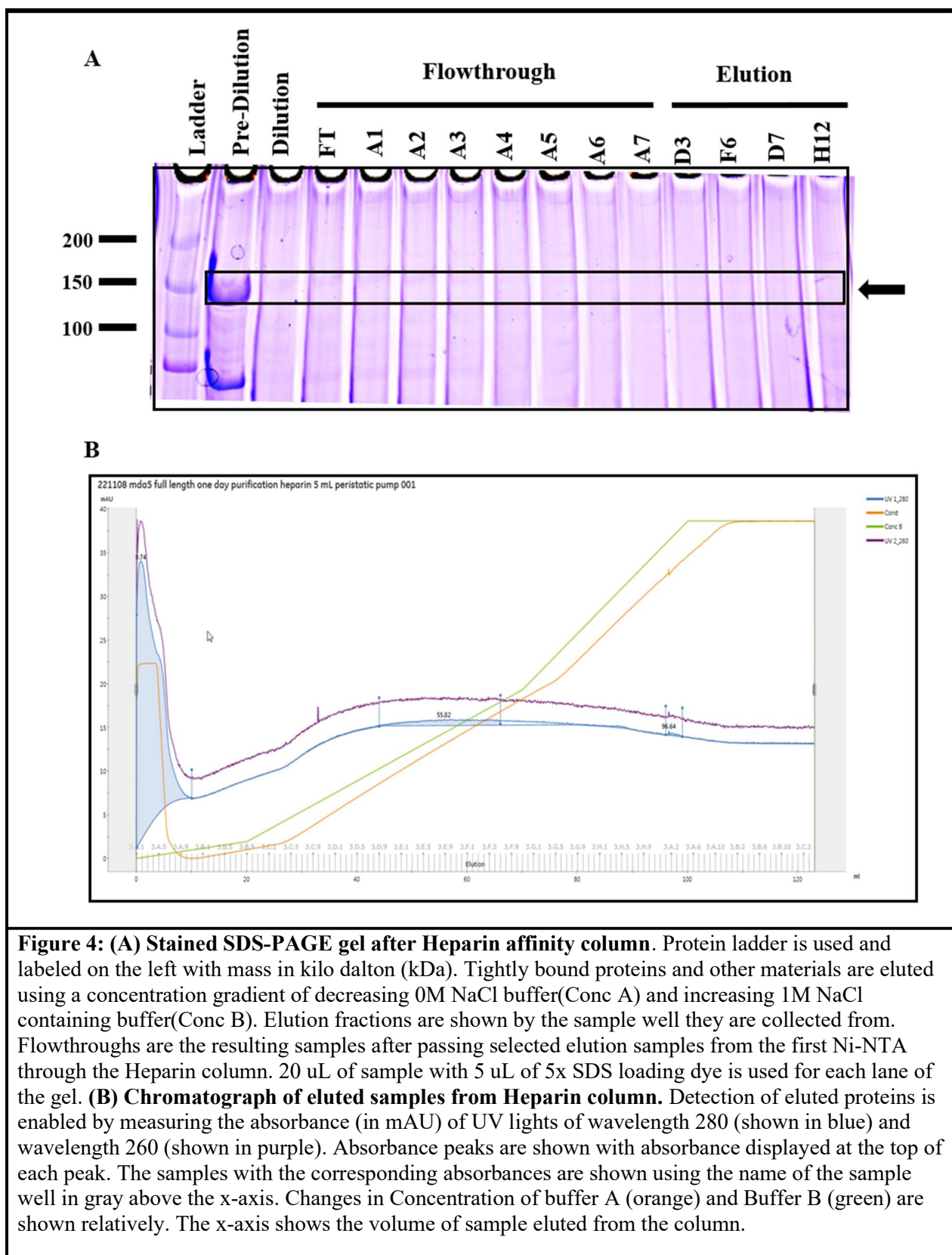


Figure 3: Stained SDS-PAGE gel after first Ni-NTA gravity column. Protein ladder is used and labeled on the left with mass in kilo dalton (kDa). Proteins bound with high affinity to the column are eluted with the elution buffer described in the method of varying imidazole concentration. Elution fractions are shown with different concentrations of imidazole in millimolar (mM). MDA5 full-length is shown as the eluting bands near at 120kDa. Wash solutions described in the method are used to elute unspecific binding elements and protein. L is the supernatant obtained after cell lysis. FT is the resulting supernatant after it is passed through the column. Pellet denotes the pellet sample from cell lysis. 20 uL of sample with 5 uL of 5x SDS loading dye is used for each lane of the gel.

Heparin Column

We attempted further purification using Heparin column which is designed for DNA/RNA binding protein purification. The diluted sample from the first Ni-NTA column was passed through a 5mL Heparin column. However, SDS-PAGE gel result shows lost of almost all full-length MDA5 after dilution as the prominent band at 120kDa in the pre-dilution sample is only faintly observable in the dilution (Figure 4A). The chromatograph supports the gel result as there is no clear absorption peak observed at either wavelength in the chromatograph (Figure 4B).



Size Exclusion Column (SEC)

Some of the elution fractions containing MDA5 from the first Ni-NTA column were stored in -80°C . We used the stored sample for size exclusion chromatography in order to further purify the sample without Heparin. We also passed the flowthrough samples from Heparin in order to confirm whether the faint bands we saw near 150kDa in Figure 4A is MDA5 or just merely smears from the SDS loading dye. The result from SDS-PAGE gel indicates that there was not a band for MDA5 full length in the flowthrough fractions of the Heparin column. This meant that all full-length MDA5 was lost during dilution. We observed the band representing full-length MDA5 full length in the stored elution sample of the first Ni-NTA. However, this band disappears in the fractions that passed through the size exclusion column. At the same time, we observed an increase in the intensity of the contaminant band at 75 kDa and the contaminant band in between 75kDa and 50 kDa in the elution fractions compared to the samples before SEC (Figure 5A). The chromatograph of the column supported this finding as we observed a high-intensity peak at the fractions where we observed intense bands in the SDS-PAGE gel (Figure 5B). These observations suggested that full-length MDA5 is highly unstable and degrades after experiencing changes from freezing temperature to room temperature. The increase in the intensity of contaminant bands was most likely a result from the degradation of full-length MDA5 into smaller peptide chains. However, the contaminant bands around 75 kDa could also be unspecific proteins that were trapped by the SEC matrix.

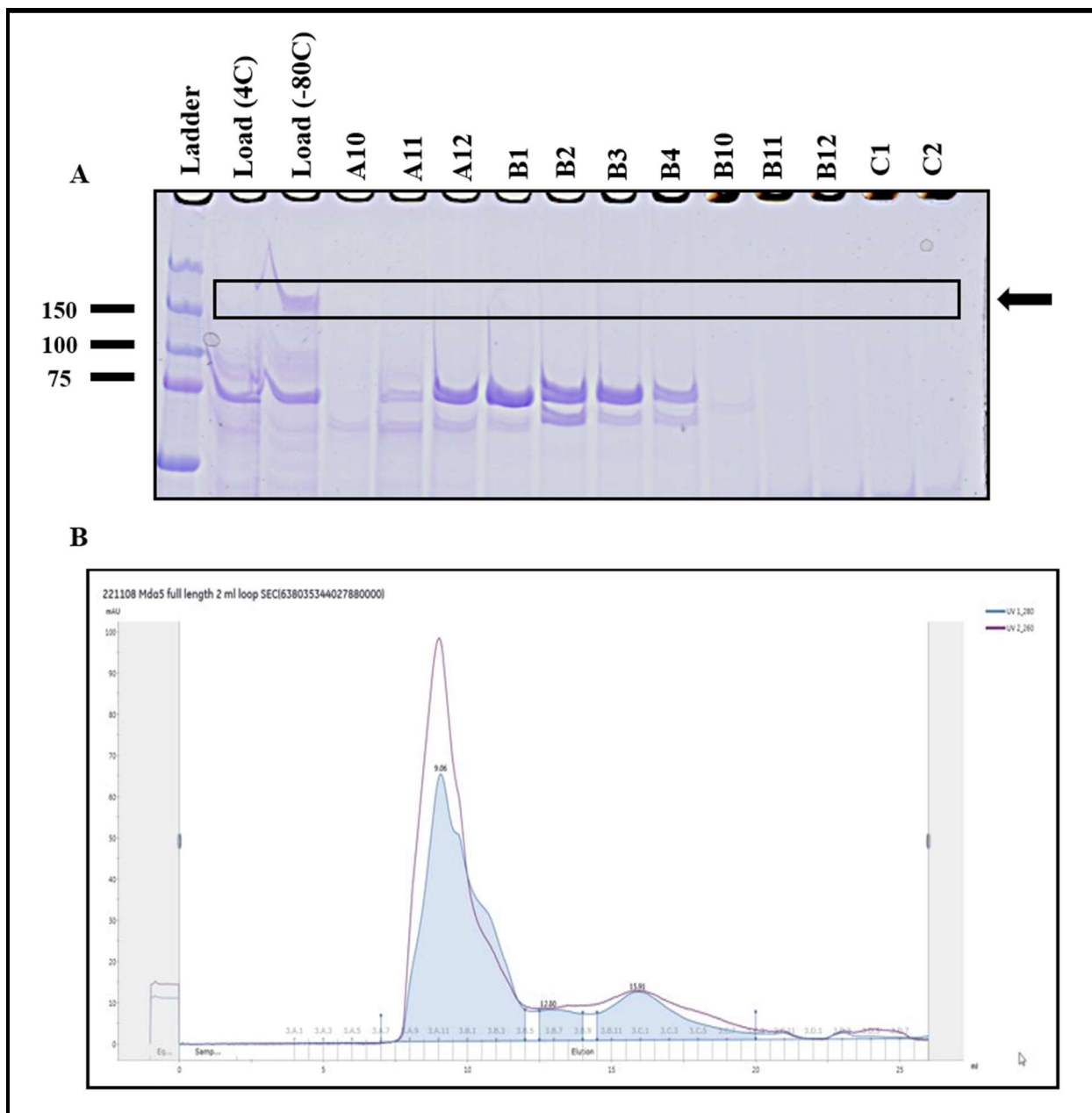


Figure 5: (A) Stained SDS-PAGE gel after SEC. Protein ladder is used and labeled on the left with mass in kilo dalton (kDa). Samples from elution fractions containing MDA5 full length (Load (-80C)) and flowthrough sample from Heparin column (Load (4C)) are passed through SEC. Elution fractions are shown by the sample well they are collected from. 20 uL of sample with 5 uL of 5x SDS loading dye is used for each lane of the gel. **(B) Chromatograph of eluted samples from SEC column.** Detection of eluted proteins is enabled by measuring the absorbance (in mAU) of UV lights of wavelength 280 (shown in blue) and wavelength 260 (shown in purple). Absorbance peaks are shown with volume of the samples in the peak at the top of each peak. The samples with the corresponding absorbances are shown using the name of the sample well in gray above the x-axis. The x-axis shows the volume of sample eluted from the column.

MDA5 CARDS purification

Ni-NTA Column

Due to issues with the purification of MDA5 full-length, we decided to purify the CARDS of the MDA5 protein (25kDa) in order to test potential binding of NS2 at these domains. Observations from SDS-PAGE gel shows positive results in the initial purification of MDA5 CARDS. The protein begins eluting at 50 mM imidazole concentration. MDA5 CARDS were overexpressed at high amount as shown by the intense bands at 25kDa which represent MDA5 CARDS with His-tag. However, the fractions containing MDA5 CARDS contain many contaminant bands including a very prominent band in between 25kDa and 37 kDa (Figure 6). Elution fractions at 400mM to 500mM imidazole are collected and combined for further purification.

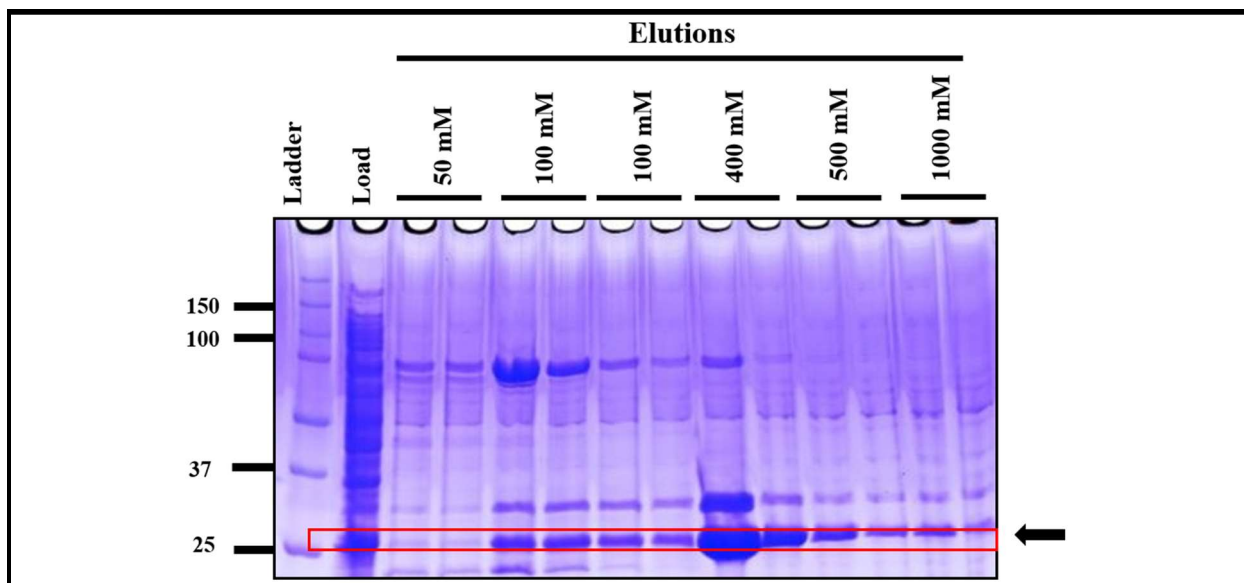


Figure 6: Stained SDS-PAGE gel after first Ni-NTA gravity column. Protein ladder is used and labeled on the left with mass in kilo dalton (kDa). The bands representing MDA5 CARDS are indicated by the red rectangle and an arrow. Proteins bound with high affinity to the column are eluted with the elution solution described in the method section with varying imidazole and NaCl concentration. Elution fractions are shown with different concentrations of imidazole in millimolar (mM). Load is the supernatant obtained after cell lysis. 20 uL of sample with 5 uL of 5x SDS loading dye is used for each lane of the gel.

Q HP Anion Exchange Affinity Column

We further purified the collected fractions from the first Ni-NTA column using Q anion exchange column. At buffer pH of 7.4, MDA5 CARDS carried an overall negative charge. The column we used had a positive charge that enables MDA5 CARDS to preferably bind to the column. Elution of MDA5 CARDS was enabled using an increasing salt concentration. SDS-PAGE gel result showed elution of MDA5 CARDS through intense bands at 25kDa in elution fractions B11, C5, C11, D7 and F5 (Figure 7A). The chromatograph supported the gel result as an intense peak with an absorbance of around 225 mAU observed at the positions of the elution samples (Figure 7B). The presence of MDA5 CARDS bands in the flowthrough fractions can be explained as the amount of protein in the collected fraction exceeded the column's binding capacity. The intensity of the MDA5 CARDS band in the elution fractions indicated high-affinity binding of MDA5 CARDS to the column. Elution F5 was shown to contain MDA5 CARDS without any contaminant band. All other elution fraction contains contaminant bands. However, it is worth noting that the relative intensity of the contaminant bands decreased compared to the intensity of the MDA5 CARDS band.

NS2-MBP purification

First Ni-NTA Column

In order to purify NS2, we use a combination tag composed of MBP and 10 histidines. MBP is tag well-known for its improvement of expressed protein's stability and solubility. Observations from SDS-PAGE gel shows positive result in the initial purification of NS2-MBP. The protein begins eluting at 100 mM imidazole concentration. NS2-MBP is overexpressed at high concentration as shown by the intense bands at 60kDa. However, the fractions containing MDA5 CARDS contain many contaminant bands (Figure 6). However, these contaminant bands are relatively lower in intensity. Elution fractions at 100mM and 400mM imidazole are collected and combined for further purification.

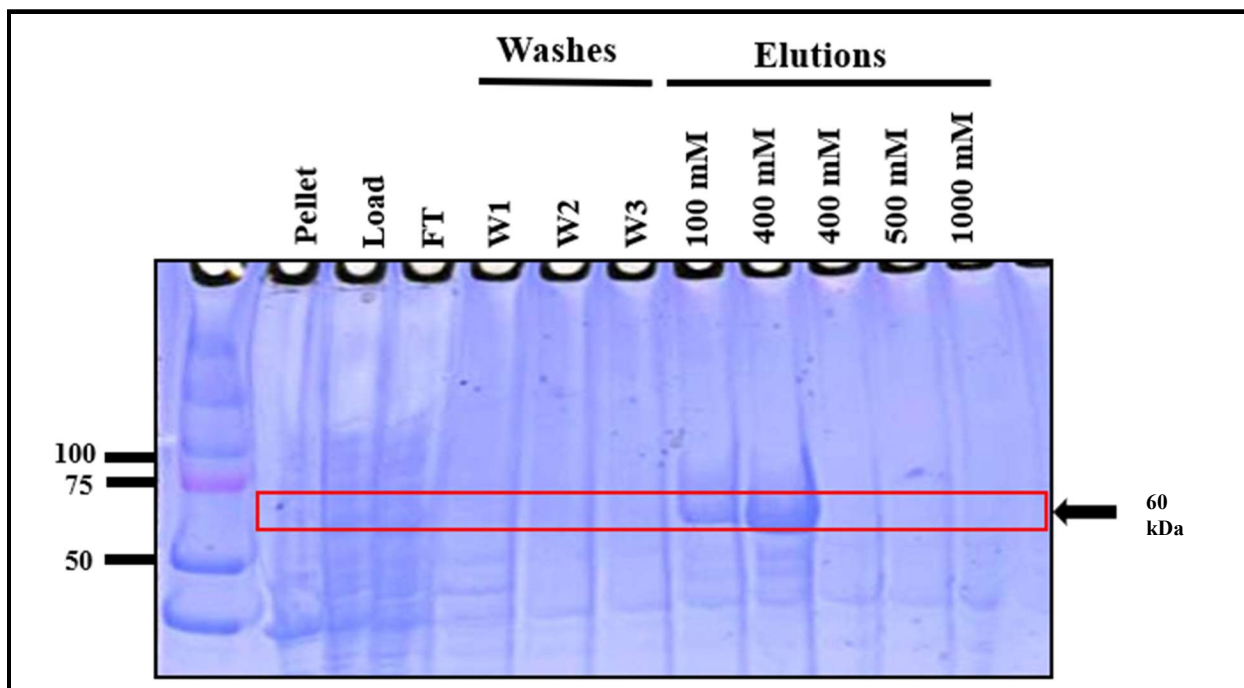
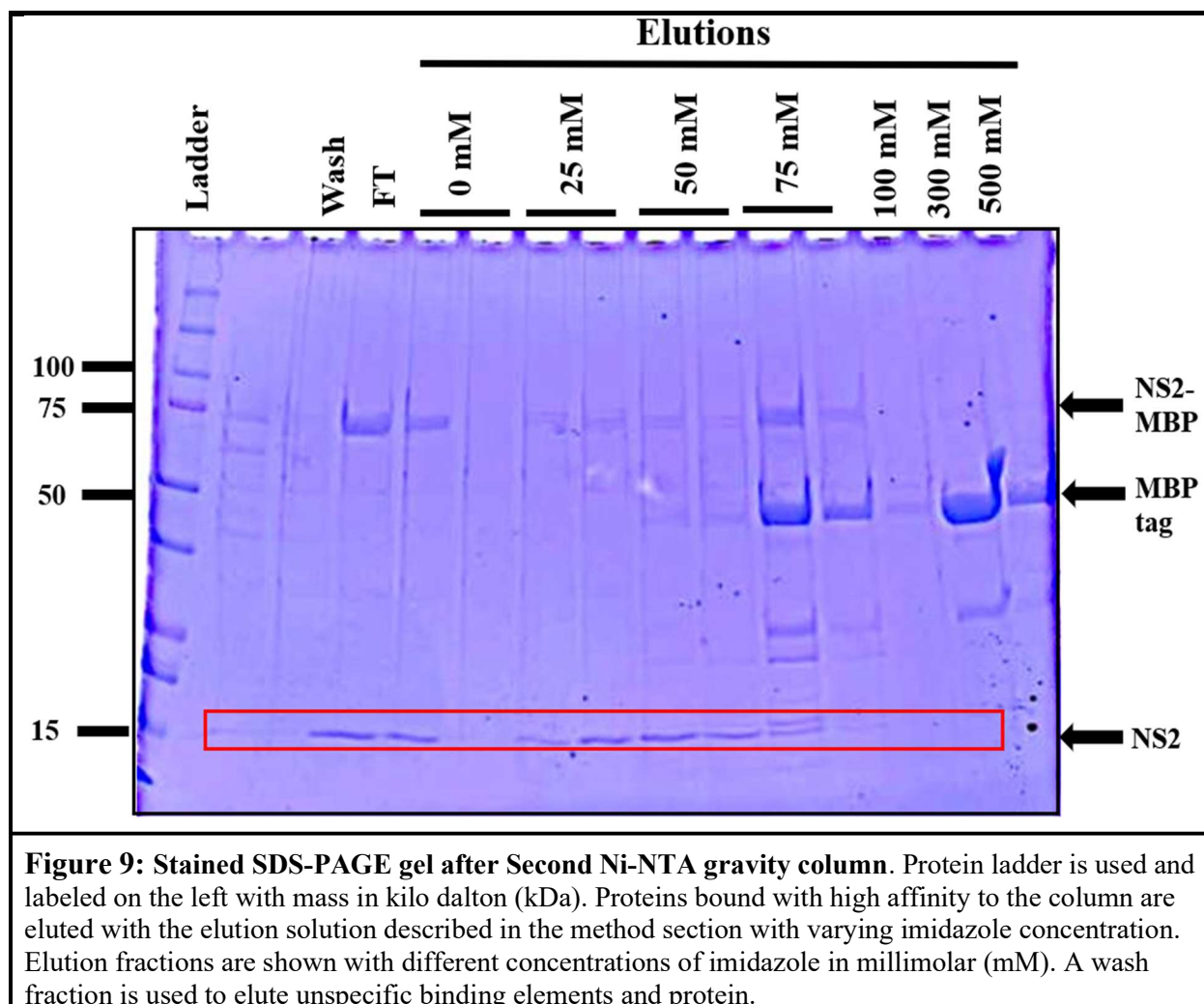


Figure 8: Stained SDS-PAGE gel after first Ni-NTA gravity column. Protein ladder is used and labeled on the left with mass in kilo dalton (kDa). Proteins bound with high affinity to the column are eluted with the elution solution described in the method section with varying imidazole concentration. Elution fractions are shown with different concentrations of imidazole in millimolar (mM). W1-W3 are wash steps in which wash solutions are used to elute unspecific binding elements and protein. Load is the supernatant obtained after cell lysis. FT is the resulting supernatant after it is passed through the column.

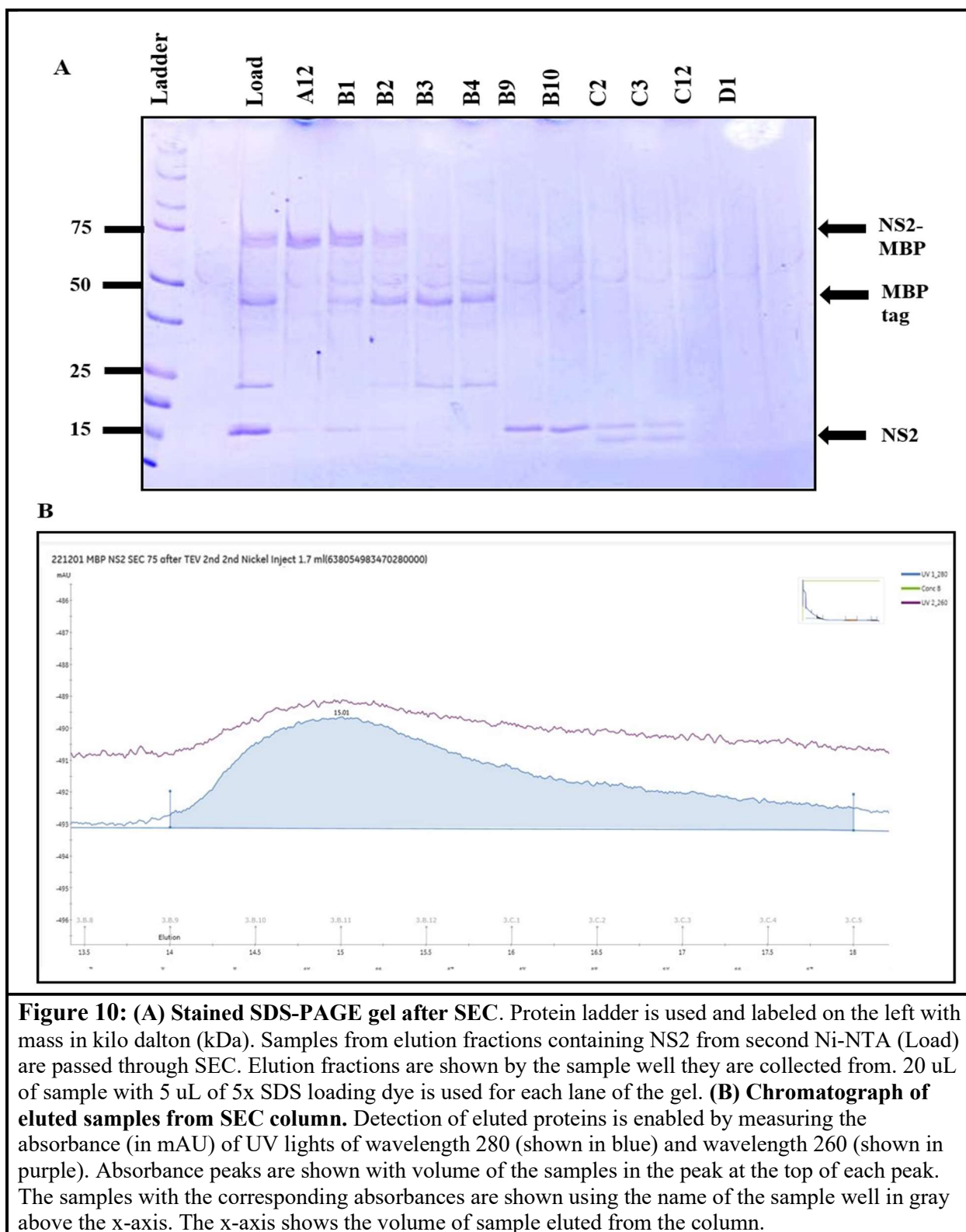
TEV cleavage and Second Ni-NTA

Elution fractions collected from the first Ni-NTA were combined and dialyzed in a 10-times-dilution in order to reduce imidazole and salt concentration. At the same time of the dialysis the sample was digested with TEV in 1:50 mass ratio in order to cleave the attached tag from NS2. The resulting sample is expected to contain the NS2 protein with cleaved MBP tag. The resulting sample after TEV treatment was passed through a second Ni-NTA column. We expect the NS2 protein without MBP tag would have less affinity toward the Ni resin and elute at a much lower imidazole concentration. The result from SDS-PAGE gel showed that the cleaved NS2 eluted at a much lower concentration of imidazole as indicated by the cleaved NS2 band at 15kDa starting from the flowthrough fraction until 50mM imidazole elution fraction. Some NS2 remained with the MBP tag as indicated by the band near 75 kDa (Figure 9). Despite failing to separate uncleaved NS2 with cleaved NS2, the column was able to separate MBP tag from cleaved NS2 as the MBP tag elutes at higher imidazole concentrations.



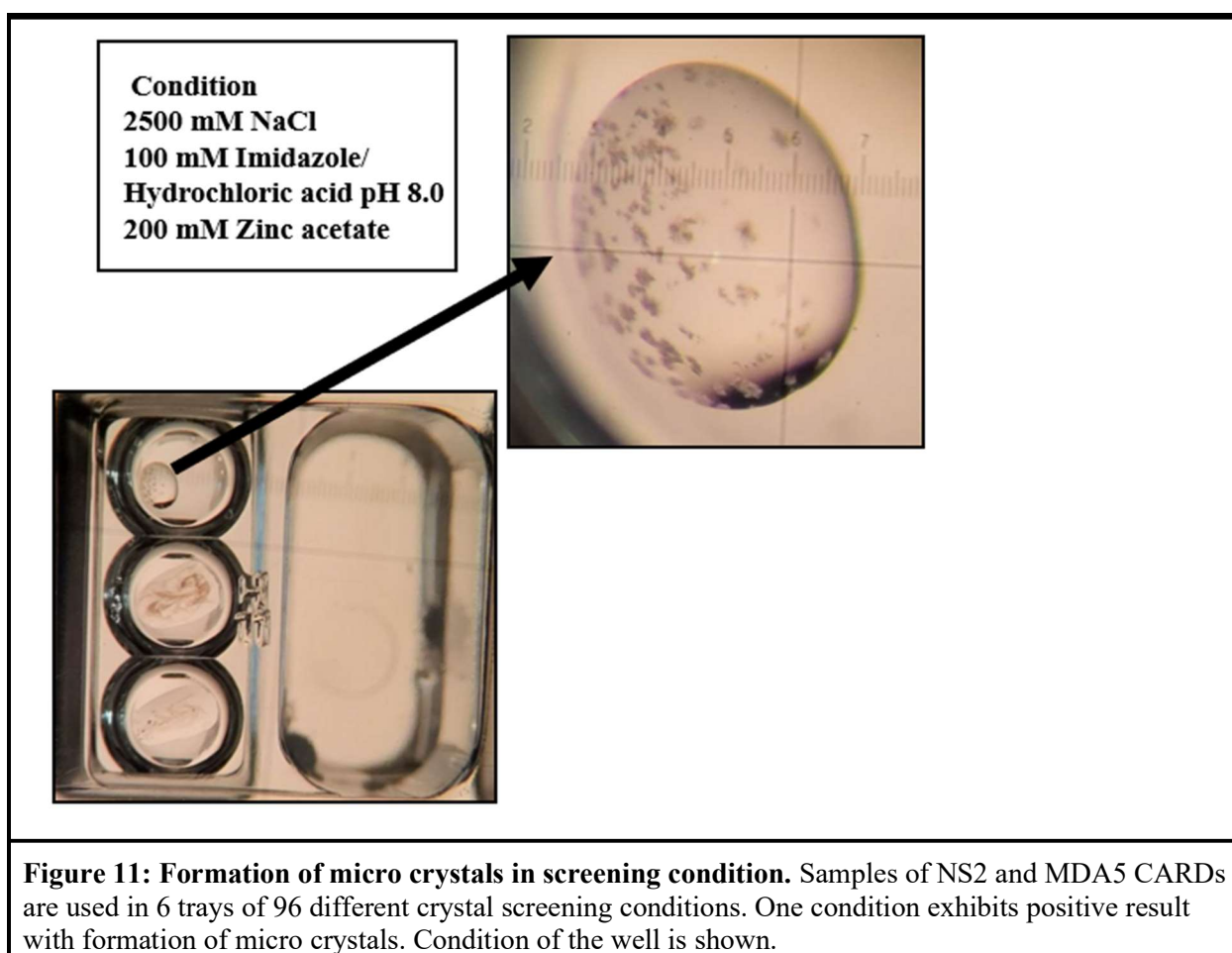
Size Exclusion Column (SEC)

Elution fractions of 25mM and 50 mM imidazole from the second Ni-NTA were passed through the size exclusion column. SDS-PAGE gel result showed separation of cleaved NS2 from NS2-MBP and MBP in elution fractions B9, B10, C2, and C3 (Figure 10A). However, there was a new contaminant band below 25kDa for fraction C2 and C3. We suspect that this can be a product of NS2 degradation or contamination of the column from prior use. There was a faint, negligible contaminant band at 50kDa. The chromatograph supported findings of the gel as a peak was observed in the elutions where the separation of NS2 is achieved (Figure 10B).



Crystal Conditions Screening

We mixed purified NS2 and MDA5 CARDS in a 1:1 mass ratio. Next, we tested for multiple crystallization conditions at various conditions of varying salt, pH, metal concentrations. The majority of our conditions formed aggregate. One condition at well H11 was able to form micro crystals, suggesting that highly ordered complexes are potentially being formed by NS2 and MDA5 CARD. However, the condition is not sufficient to form a crystal suitable for structural studies using X-ray diffraction.



Discussion and Future Direction

In order to study the structural antagonism of RSV viral protein NS2 on human RIG-I and MDA5, we sought to optimize the expression and purification system of the proteins in question using *Escherichia coli*. We were able to successfully overexpress and purify NS2 and MDA5 CARDS with minimal contaminants. Additional large-scale purifications of NS2 and MDA5 CARDS will be necessary to generate samples for our future structural studies. Next, we will need to create and optimize a purification protocol to obtain samples of full-length RIG-I. In the event that purification of full-length RIG-I fails, we can purify RIG-I CARDS domain instead as NS2 is found to interact with RIG-I at its CARD domain ⁽²⁾.

Our attempts at purifying full-length MDA5 were not successful due to the instability of the full-length MDA5 expressed by *E. coli* BL21 cells. In order to successfully purify full-length MDA5 in the future, we need to improve its stability. It is well established in scientific literature that MDA5 forms filaments along double-stranded RNA ^(13, 14). The interaction with double stranded RNA may improve the stability of MDA5. Therefore, we can add double stranded RNA into elution fractions containing MDA5 after the first Ni-NTA column before moving to the next purification step in future purification attempts.

Initial crystal condition screening shows a potential condition for crystal formation with the formation of micro crystals (Figure 11). Moving forward, we should optimize the condition by modifying the components of the identified potential conditions and testing different combinations using the hanging drops method. Another way to increase our chance of forming crystal is to improve the purity of our protein samples. This would require further optimization of

our purification methods. After a suitable condition is found and a crystal of the complex between NS2 and MDA5 CARDS is formed, we can move on to study the structure of this interaction through X-ray crystallography. The resulting structure of the interaction could be extremely valuable in designing future therapeutic against RSV and improve our understanding of NS2 structural functions.

Materials and Methods

Cells and Plasmids

Proteins for this study were expressed using *Escherichia coli* BL21(DE3). We used 2CT-10 plasmid for our NS2 MBP construct, 2BT-10 plasmid for our MDA5 CARDS construct. Details of our plasmids with restriction sites are included in the figure below.

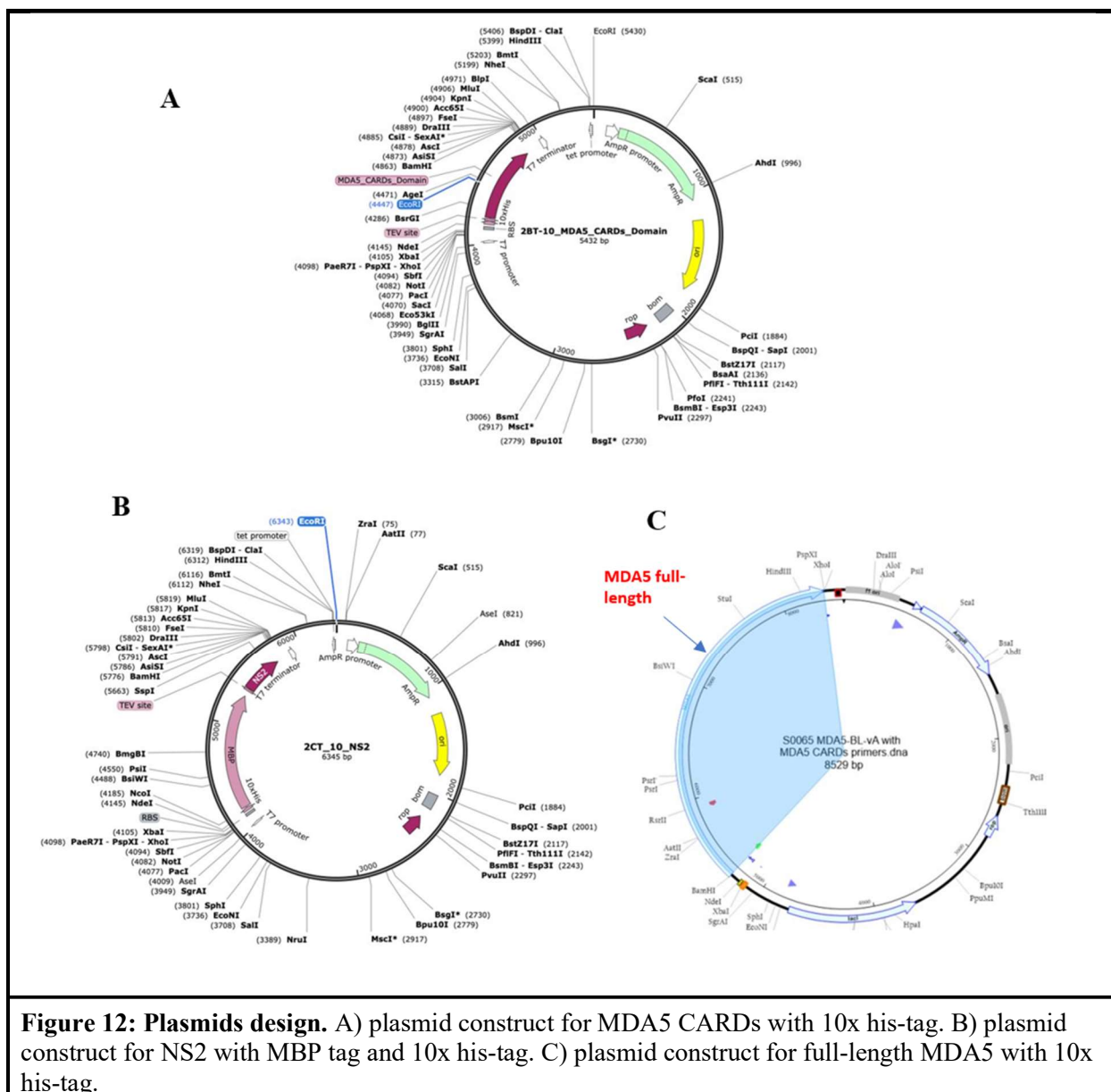


Figure 12: Plasmids design. A) plasmid construct for MDA5 CARDS with 10x his-tag. B) plasmid construct for NS2 with MBP tag and 10x his-tag. C) plasmid construct for full-length MDA5 with 10x his-tag.

Transformation

Competent *E. coli* BL21(DE3) cells were mixed with plasmids containing the desired recombinant protein in the following ratio: 200ng plasmid / 50 μ L cell (MDA5 full length); 200ng plasmid / 50 μ L cell (MDA5 CARDS); 200ng plasmid / 50 μ L cell (NS2). The mixture was incubated on ice for 30 minutes. Uptake of the plasmid by the *E. coli* cells were induced through heat shock at 42°C for 45 seconds. The mixture was then cooled on ice for 5 minutes. 900 μ L of LB was added to the mixture and incubated in a shaker at 37°C for growth in 1 hour. 100 μ L of the mixture was plated onto a cell culture agar plate containing 100 mM carbenicillin. The plate was incubated at 37°C overnight.

Protein expression

The transformed cell colonies were grown in 250mL Luria broth mediums with 1:1000 ratio of Ampicillin (250 μ L). The mediums were grown overnight at 37°C. The mediums were transferred into 1L flasks for further growth (10mL per 1-L flask) at 37°C. Once the OD₆₀₀ of each flask reached 0.4–0.6, the flasks were cooled on ice and induced with 500mM isopropyl β -D-1-thiogalactopyranoside (IPTG). The temperature of the shaker was lowered to 20°C. The flasks were incubated overnight for protein expression.

Protein purification

Cell from Luria broth culture was harvested by centrifugation at 3800 rounds per minute (rpm) for 30 minutes at 4°C. Resulting cell pellets from each 1L culture were washed with deionized water and resuspended in 50 mL lysis buffer (25mM Na₃PO₄ pH 7.4, 500mM NaCl, 10% glycerol, 2mM β -mercaptoethanol). Resuspended cells were mixed with protease inhibitors in the following amount: 500 μ L phenylmethylsulfonyl fluoride (PMSF); 50 μ L Aprotinin; 50 μ L Pepstatin; 50 μ L Leupeptin. The mixture was sonicated on ice at 50% amplitude for 20 minutes.

The supernatant of the lysate was separated using high speed centrifugation at 18000 rpm for 1 hour at 4°C. The supernatant was then incubated in Ni-NTA resin equilibrated with the lysis buffer (first Ni-NTA column). The resin was then washed with wash buffers (25mM Na₃PO₄ pH 7.4, 750mM NaCl, 10% glycerol, 2mM β-mercaptoethanol, 50mM – 75mM imidazole) in a gravity column. The proteins were eluted using an elution buffer (25mM Na₃PO₄ pH 7.4, 150mM NaCl, 10% glycerol, 2mM β-mercaptoethanol, 200mM – 600mM imidazole). The column was then cleaned with 15mL of 25mM Na₃PO₄ pH 7.4, 150mM NaCl, 10% glycerol, 2mM β-mercaptoethanol, 1M imidazole. Fractions containing the desired protein were dialyzed with 25mM HEPES pH 7.4, 150mM NaCl, 10% glycerol, 2mM β-mercaptoethanol. At the time of the dialysis, the fractions were digested with TEV protease at the mass ratio of 1:20. The resulting fractions were put through a second Ni-NTA gravity column. The flowthrough fraction is expected to contain the desired protein and was collected for concentration using concentrator of the appropriate molecular cut-off point. The protein containing fraction was concentrated to around 2mL and was further purified through a different type of affinity column or size exclusion column using the ÄKTA™ pure protein purification system.

References

1. Center of Disease Control and Prevention, USA. <https://www.cdc.gov/rsv/index.html>.
2. Ling Z, Tran KC, Teng MN. Human respiratory syncytial virus nonstructural protein NS2 antagonizes the activation of beta interferon transcription by interacting with RIG-I. *J Virol*. 2009 Apr;83(8):3734-42. doi: 10.1128/JVI.02434-08. Epub 2009 Feb 4. PMID: 19193793; PMCID: PMC2663251.
3. Onomoto, K., Onoguchi, K. & Yoneyama, M. Regulation of RIG-I-like receptor-mediated signaling: interaction between host and viral factors. *Cell Mol Immunol* **18**, 539–555 (2021). <https://doi.org/10.1038/s41423-020-00602-7>.
4. Schobel, S., Stucker, K., Moore, M. *et al*. Respiratory Syncytial Virus whole-genome sequencing identifies convergent evolution of sequence duplication in the C-terminus of the G gene. *Sci Rep* **6**, 26311 (2016). <https://doi.org/10.1038/srep26311>
5. Kotelkin A, Belyakov IM, Yang L, Berzofsky JA, Collins PL, Bukreyev A. The NS2 protein of human respiratory syncytial virus suppresses the cytotoxic T-cell response as a consequence of suppressing the type I interferon response. *J Virol*. 2006 Jun;80(12):5958-67. doi: 10.1128/JVI.00181-06. Erratum in: *J Virol*. 2006 Oct;80(20):10286. PMID: 16731934; PMCID: PMC1472589.
6. Lo MS, Brazas RM, Holtzman MJ. Respiratory syncytial virus nonstructural proteins NS1 and NS2 mediate inhibition of Stat2 expression and alpha/beta interferon responsiveness. *J Virol*. 2005 Jul;79(14):9315-9. doi: 10.1128/JVI.79.14.9315-9319.2005. PMID: 15994826; PMCID: PMC1168759.

7. Ramaswamy M, Shi L, Monick MM, Hunninghake GW, Look DC. Specific inhibition of type I interferon signal transduction by respiratory syncytial virus. *Am J Respir Cell Mol Biol*. 2004 Jun;30(6):893-900. doi: 10.1165/rcmb.2003-0410OC. Epub 2004 Jan 12. PMID: 14722224.
8. Schlender J, Bossert B, Buchholz U, Conzelmann KK. Bovine respiratory syncytial virus nonstructural proteins NS1 and NS2 cooperatively antagonize alpha/beta interferon-induced antiviral response. *J Virol*. 2000 Sep;74(18):8234-42. doi: 10.1128/jvi.74.18.8234-8242.2000. PMID: 10954520; PMCID: PMC116331.
9. Kowalinski E, Lunardi T, McCarthy AA, Louber J, Brunel J, Grigorov B, Gerlier D, Cusack S. Structural basis for the activation of innate immune pattern-recognition receptor RIG-I by viral RNA. *Cell*. 2011 Oct 14;147(2):423-35. doi: 10.1016/j.cell.2011.09.039. PMID: 22000019.
10. Jiang F, Ramanathan A, Miller MT, Tang GQ, Gale M Jr, Patel SS, Marcotrigiano J. Structural basis of RNA recognition and activation by innate immune receptor RIG-I. *Nature*. 2011 Sep 25;479(7373):423-7. doi: 10.1038/nature10537. PMID: 21947008; PMCID: PMC3430514.
11. Pichlmair A, Schulz O, Tan CP, Näslund TI, Liljeström P, Weber F, Reis e Sousa C. RIG-I-mediated antiviral responses to single-stranded RNA bearing 5'-phosphates. *Science*. 2006 Nov 10;314(5801):997-1001. doi: 10.1126/science.1132998. Epub 2006 Oct 12. PMID: 17038589.
12. Kolakofsky D, Kowalinski E, Cusack S. A structure-based model of RIG-I activation. *RNA*. 2012 Dec;18(12):2118-27. doi: 10.1261/rna.035949.112. Epub 2012 Nov 1. PMID: 23118418; PMCID: PMC3504664.

13. Berke IC, Modis Y. MDA5 cooperatively forms dimers and ATP-sensitive filaments upon binding double-stranded RNA. *EMBO J*. 2012 Apr 4;31(7):1714-26. doi: 10.1038/emboj.2012.19. Epub 2012 Feb 7. PMID: 22314235; PMCID: PMC3321199.
14. Peisley A, Lin C, Wu B, Orme-Johnson M, Liu M, Walz T, Hur S. Cooperative assembly and dynamic disassembly of MDA5 filaments for viral dsRNA recognition. *Proc Natl Acad Sci U S A*. 2011 Dec 27;108(52):21010-5. doi: 10.1073/pnas.1113651108. Epub 2011 Dec 12. PMID: 22160685; PMCID: PMC3248507.
15. Reikine S, Nguyen JB, Modis Y. Pattern Recognition and Signaling Mechanisms of RIG-I and MDA5. *Front Immunol*. 2014 Jul 23;5:342. doi: 10.3389/fimmu.2014.00342. PMID: 25101084; PMCID: PMC4107945.
16. Liu P, Jamaluddin M, Li K, Garofalo RP, Casola A, Brasier AR. Retinoic acid-inducible gene I mediates early antiviral response and Toll-like receptor 3 expression in respiratory syncytial virus-infected airway epithelial cells. *J Virol*. 2007 Feb;81(3):1401-11. doi: 10.1128/JVI.01740-06. Epub 2006 Nov 15. PMID: 17108032; PMCID: PMC1797494.
17. Scagnolari C, Midulla F, Pierangeli A, Moretti C, Bonci E, Berardi R, De Angelis D, Selvaggi C, Di Marco P, Girardi E, Antonelli G. Gene expression of nucleic acid-sensing pattern recognition receptors in children hospitalized for respiratory syncytial virus-associated acute bronchiolitis. *Clin Vaccine Immunol*. 2009 Jun;16(6):816-23. doi: 10.1128/CVI.00445-08. Epub 2009 Apr 22. PMID: 19386802; PMCID: PMC2691037.
18. Pei, Jingjing, et al. "Structural basis for IFN antagonism by human respiratory syncytial virus nonstructural protein 2." *Proceedings of the National Academy of Sciences* 118.10 (2021): e2020587118.

19. Van Royen T, Rossey I, Sedeyn K, Schepens B, Saelens X. How RSV Proteins Join Forces to Overcome the Host Innate Immune Response. *Viruses*. 2022 Feb 17;14(2):419. doi: 10.3390/v14020419. PMID: 35216012; PMCID: PMC8874859.
20. Loo YM, Fornek J, Crochet N, Bajwa G, Perwitasari O, Martinez-Sobrido L, Akira S, Gill MA, García-Sastre A, Katze MG, Gale M Jr. Distinct RIG-I and MDA5 signaling by RNA viruses in innate immunity. *J Virol*. 2008 Jan;82(1):335-45. doi: 10.1128/JVI.01080-07. Epub 2007 Oct 17. PMID: 17942531; PMCID: PMC2224404.
21. Rehwinkel J, Gack MU. RIG-I-like receptors: their regulation and roles in RNA sensing. *Nat Rev Immunol*. 2020 Sep;20(9):537-551. doi: 10.1038/s41577-020-0288-3. Epub 2020 Mar 13. PMID: 32203325; PMCID: PMC7094958.